

Asphericity of the base of the solar convection zone

SARBANI BASU¹ AND SYLVAIN G. KORZENNIK²

¹*Department of Astronomy, Yale University, PO Box 208101, New Haven, CT 06520-8101, USA*

²*Center for Astrophysics | Harvard & Smithsonian, Cambridge, MA 02138, USA*

ABSTRACT

We have used solar oscillation frequencies and frequency splittings obtained over solar cycles 23 and 24 to investigate whether the base of the solar convection zone shows any departure from spherical symmetry. We used the even-order splitting coefficients, a_2 – a_8 , and estimated the contributions from each one separately. The average asphericity over the two solar cycles was determined using frequencies and splittings obtained with a 9216-day time-series. We find that evidence of asphericity is, *at best*, marginal: the a_2 component is consistent with no asphericity, the a_4 and a_6 components yield results at a level a little greater than 1σ , while the a_8 component shows a signature below 1σ . The combined results indicate that the time average of the departure from the spherically symmetric position of the base of the convection zone is $\lesssim 0.0001R_\odot$. We have also used helioseismic data obtained from time-series of lengths 360 days, 576 days, 1152 days, and 2304 days in order to examine the consistency of the results and evaluate whether there is any time variation. We find that the evidence for time variation is statistically marginal in all cases, except for the a_6 component, for which tests consistently yield p values of less than 0.05.

Keywords: The Sun (1693) — Helioseismology (709) — Solar interior (1500) — Solar convective zone(1998) — Solar cycle (1487)

1. INTRODUCTION

The base of the solar convection zone (henceforth CZ) marks the position where the thermal gradient changes from being radiative in the interior to adiabatic in the outer layers. The position where this change happens is known very well (e.g., Christensen-Dalsgaard et al. 1991; Basu & Antia 1997; Basu 1998). It is determined assuming that the base is spherically symmetric. In fact, the position of the CZ base is a test of the physics used in constructing solar models (e.g., Christensen-Dalsgaard et al. 1993).

The base of the CZ is also where the solar tachocline is located. This is a narrow shear layer that marks the change from latitudinal differential rotation in the CZ to a solid body rotation in the interior. The tachocline however, is prolate in shape (Antia et al. 1998; Charbonneau et al. 1999); at the equator this layer is centered below the CZ base, while at a lati-

tude of 60° , it is above the CZ base. This raises the question, whether the base of the CZ is indeed spherically symmetric. Spiegel & Zahn (1992) noted that the tachocline could drive meridional flows. It has been argued (Gough & Kosovichev 1995) that these flows must affect the thermal balance of the layers, and could influence where the layer becomes unstable to convection, thereby causing the base of the CZ to deviate from spherical symmetry.

Rotation is expected to make the CZ base oblate, though the expected oblateness is small — the surface value of the difference between equatorial and polar radius is only a few parts in 10^6 (Kuhn et al. 2012), the rotation rate at the CZ base is not much different. Another expected cause of any asphericity of the CZ base, is the magnetic field that might be there. Indeed, there may be belts of magnetic fields intense enough to modify convection. Once the magnetic fields become buoyant and rises up, convection could be enhanced by the field, thus the CZ base would exhibit time-dependent asphericity (see Gough & Kosovichev 1995).

Previous investigations on the asphericity of the CZ base give results that do not agree with one

another. Using frequencies obtained by the Big Bear Solar Observatory (Woodard & Libbrecht 1993), Gough & Kosovichev (1995) used combinations of frequencies and splitting coefficients to determine the frequencies sensitive at three different latitudes, and inverted the resulting combinations to determine the relative isothermal difference between a spherically symmetric model and that implied by the frequency combinations. They interpreted their results as a difference in the CZ base of no more than $0.02R_{\odot}$ between the pole and the equator. Monteiro et al. (2001) attempted to look for asphericity at the CZ base using data from the Michelson Doppler Imager (MDI; Scherrer et al. 1995). They fitted the signature of the acoustic “glitch” caused by the change in the thermal gradient at the CZ base to determine the acoustic depth of this feature. They found a latitude-dependent difference in the acoustic depth, of the order of 100 seconds, and a small, time dependence at low latitudes. Like Gough & Kosovichev (1995), they used combined frequencies and splittings to obtain frequencies that correspond to various latitudes, but their combinations were modified by an initial inversion to get localized latitudinal response of the combination. In contrast, Basu & Antia (2001) found a much smaller difference, and derived an upper limit of $0.0005R_{\odot}$ on the asphericity of the CZ base; they used data from the Global Oscillation Network Group (GONG; Hill et al. 1996) and the MDI and, like Gough & Kosovichev (1995), combined frequencies and splittings to obtain frequencies that represent various latitudes. Basu & Antia (2001) did not invert the frequencies, instead they used the technique developed by Basu & Antia (1997) to determine the position of the CZ base. Antia et al. (2001a, 2003) did two-dimensional inversions to determine the latitudinal dependence of solar structure, they found distinct asphericity in the outer layers, but nothing significant at the CZ base.

Much more helioseismic data are now available, and in this paper, we use helioseismic data collected over solar cycles 23 and 24 to assess whether the CZ base shows any asphericity and furthermore, whether there is any time variation of the asphericity. We use mode frequencies and splitting obtained by different projects, and more importantly, we use frequencies and frequency splittings obtained using different lengths of helioseismic time-series. Unlike all earlier attempts, we do not combine the frequencies and splittings to determine frequencies for a given latitude, but determine the contribution of each term separately and derive the uncertainty due to each term separately.

The rest of the paper is organized as follows. In Section 2 we describe how one can determine the combi-

nation of frequencies and frequency splittings in order to be sensitive to different latitudes, and in particular we describe our approach of determining the asphericity of the CZ base. In Section 3 we describe the method of determining the position of the CZ base. Section 4 describes the different data sets that we use. Our results are presented in Section 5, and our conclusions in Section 6.

2. DETERMINING ASPHERICITY

We follow the formulation presented in Antia et al. (2001b) and Basu & Antia (2001) to determine the asphericity at the base of the CZ. We use mode frequencies and their splittings, expressed in the usual manner as:

$$\nu_{nlm} = \nu_{nl} + \sum_{j=1}^{j_{\max}} a_j(n, l) \mathcal{P}_j^{(l)}(m), \quad (1)$$

where ν_{nl} , or the central frequency, is determined by the spherically symmetric part of solar structure, a_j are splitting coefficients and \mathcal{P}_j are re-scaled Clebsch-Gordon coefficients (Schou et al. 2002). In this decomposition, the odd-order a_j are caused by the solar rotation, while the even-order coefficients contain the signature of asphericity and magnetic field.

It should be noted that with global helioseismic data, one cannot distinguish between magnetic fields and asphericity (see e.g., Zweibel & Gough 1995). We chose to interpret the signature in even-order splitting coefficients as being caused by asphericity, this is what has been done in all previous estimates of asphericity from global helioseismic data.

We consider only axisymmetric perturbations in structure, with the symmetry axis coinciding with the rotation axis. Since we use global modes, our inferences, like for the rotation rate, cannot differentiate between the northern and southern hemispheres, but return estimates for a mean hemisphere. This allows us to use the variational principle and write the difference in frequency between the Sun and a solar model for a mode of a given order, spherical harmonic degree and azimuthal order (n , l , and m) as:

$$\frac{\delta\nu_{nlm}}{\nu_{nlm}} = \int_0^R dr \int_0^{2\pi} d\phi \int_0^{\pi} \sin\vartheta d\vartheta \left(\mathcal{K}_{c^2, \rho}^{nl}(r) \frac{\delta c^2}{c^2}(r, \vartheta) + \mathcal{K}_{\rho, c^2}^{nl}(r) \frac{\delta\rho}{\rho}(r, \vartheta) \right) Y_l^m (Y_l^m)^*, \quad (2)$$

where r is radius, ϑ is the co-latitude, $\delta\nu_{nlm}/\nu_{nlm}$ is the relative frequency difference, and $\mathcal{K}_{c^2, \rho}^{nl}(r)$ and $\mathcal{K}_{\rho, c^2}^{nl}(r)$ are the kernels for spherically symmetric perturbations (see e.g., Antia & Basu 1994; Kosovichev 1999). The

functions Y_l^m are spherical harmonics, denoting the angular dependence of the eigenfunctions for a spherically symmetric star, and are normalized such that

$$\int_0^{2\pi} d\phi \int_0^\pi \sin \vartheta d\vartheta Y_l^m (Y_l^m)^* = 1. \quad (3)$$

The angular integrals in Eq. 2 can be evaluated to give

$$\int_0^{2\pi} d\phi \int_0^\pi \sin \vartheta d\vartheta Y_l^m (Y_l^m)^* P_{2k}(\cos \vartheta) = \frac{1}{l} Q_{lk} \mathcal{P}_{2k}^{(l)}(m) \quad (4)$$

where Q_{lk} depends only on l, k and $\mathcal{P}_{2k}^{(l)}(m)$ are the orthogonal polynomials defined in Eq. 1. The extra factor of $1/l$ ensures that Q_{lk} approach a constant value at large l .

With this choice of expansion, the inversion problem can be decomposed into independent inversions for each even splitting coefficient, a_{2k} , and $\delta c^2/c^2$ and $\delta\rho/\rho$ can be expressed in terms of the even order Legendre polynomials, P_i :

$$\frac{\delta c^2}{c^2}(r, \vartheta) = \sum_k \left(\frac{\delta c^2}{c^2}\right)_k(r) P_{2k}(\cos \vartheta), \quad (5)$$

and,

$$\frac{\delta\rho}{\rho}(r, \vartheta) = \sum_k \left(\frac{\delta\rho}{\rho}\right)_k(r) P_{2k}(\cos \vartheta). \quad (6)$$

Thus, $(\delta c^2/c^2)_k(r)$ and $(\delta\rho/\rho)_k(r)$ can be computed by inverting each of the splitting coefficient a_{2k} . Note that this is similar to the ‘‘1.5D’’ inversions used to infer the rotation rate, where a two-dimensional solution is obtained from a series of one dimensional inversions:

$$\frac{la_{2k}(n, l)}{\nu_{nl} Q_{lk}} = \int_0^R \mathcal{K}_{c^2, \rho}^{nl} c_k(r) dr + \int_0^R \mathcal{K}_{\rho, c^2}^{nl} \rho_k(r) dr. \quad (7)$$

Instead of determining the CZ base at different colatitudes from the corresponding frequency difference, we estimate the difference in CZ over the spherically symmetric value implied by the different orders of the even-order coefficients separately; we do this for a_2 – a_8 ; higher order coefficient have large uncertainties and hence, we do not use those. In other words, we take the combination

$$\delta\nu = \delta\nu_{nl} + \frac{la_{2k}(n, l)}{Q_{lk}} \quad (8)$$

for $k = 1, 2, 3$, and 4 separately, determine the position of the CZ base in each case, and then subtract the CZ

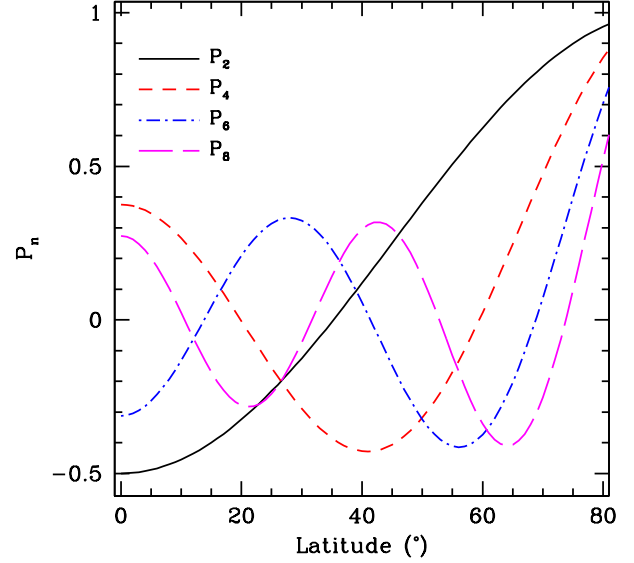


Figure 1. $P_{2k}(\cos \vartheta)$ plotted as a function of latitude θ , to show how different even-order a -coefficients contribute to the asphericity of the CZ base. Thus, for example, if $\Delta R_{CZ}(a_2)$ is positive, the CZ base at the equator will be deeper than that at higher latitudes, making it prolate.

base implied by $\delta\nu_{nl}$ to obtain $\Delta R_{CZ}(a_{2k})$ for each a_{2k} under consideration. Adding $\delta\nu_{nl}$ is necessary for our method (see Section 3), which relies on determining the frequency differences between models with known CZ depth and the Sun to work properly. Once we have estimates of ΔR_{CZ} for each case, they are combined to obtain the CZ base at any given co-latitude, i.e.,

$$R_{CZ}(\vartheta) = R_{CZ}(\nu) + \sum_k \Delta R_{CZ}(a_{2k}) P_{2k}(\cos \vartheta), \quad (9)$$

where $R_{CZ}(\nu)$ is the spherically symmetric part of the CZ base obtained using the central frequencies, and $\Delta R_{CZ}(a_{2k})$ is the contribution of a given even-order a -coefficient. We determine $\Delta R_{CZ}(a_{2k})$ for $k = 1, 2, 3$ and 4 separately using the data combinations in Eq. 8, and subtract the spherically symmetric part of the CZ base. We do not use higher-order a coefficients since the uncertainties in those are very large, in fact, as we will see later in § 5, the uncertainties even in a_8 are large enough to mask out any signs of asphericity. In the rest of the paper, when we talk of ‘‘asphericity’’ we refer to, depending on the context, either $\Delta R_{CZ}(a_{2k})$ or $R_{CZ}(\vartheta)$.

In Fig. 1, we illustrate P_{2k} as a function of latitude. The figure shows that a positive $\Delta R_{CZ}(a_2)$ implies that the CZ base at the equator is deeper than that at the higher latitudes, namely that the CZ base is prolate. Of course, higher-order contributions make the shape more complex.

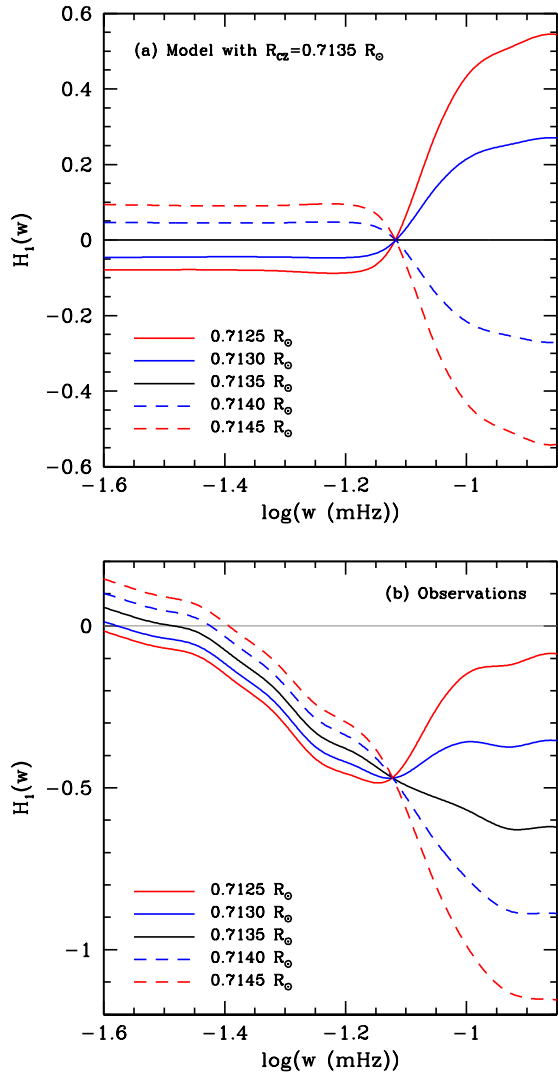


Figure 2. The function $H_1(w)$ between a (a) solar envelope model and (b) solar frequencies and solar envelope models with different CZ positions. The test solar model in panel (a) has the same physics as the calibration models. The observational data used in panel (b) is an HMI set obtained with a 2304-day time-series with a start date of 2001.08.11. Note the need for the term $H_s(w)$ in Eq. 11 in order to fit the curves in panel (b) with those in panel (a).

3. ESTIMATING THE POSITION OF THE CZ BASE

We use the method developed and used by Basu & Antia (1997); Basu (1998) to determine the position of the CZ base, that can be summarized as follows. If there are two otherwise similar solar models with different depths of the convection zone, then just below the base of the convection zone the model with a deeper convection zone will have a larger sound speed than the other. This observable difference of sound

speeds can be calibrated to find the convection zone depth of a test model or the Sun, as was first done by Christensen-Dalsgaard et al. (1991).

Asymptotically, the frequency differences between a solar model and the Sun, or between two solar models can be written as (Christensen-Dalsgaard et al. 1989)

$$S(w) \frac{\delta\omega}{\omega} = H_1(w) + H_2(w), \quad (10)$$

where $w = \omega/(l + 0.5)$, $\omega = 2\pi\nu$, and $S(w)$ is a known function for a given reference model. The functions $H_1(w)$ and $H_2(w)$ can be determined by a least-squares fit to the known frequency differences. The function H_2 contains the contribution from the “surface term,” i.e., the contribution from our inability to model the near-surface layers of the Sun properly. $H_1(w)$ can be inverted to obtain the sound-speed difference, $\delta c/c$, between the reference model and the Sun. However, Basu & Antia (1997) showed that that is not required, since $H_1(w)$ itself can be used to determine the convection-zone depth.

If $\phi(w)$ is the $H_1(w)$ between two solar models which differ only in the depth of the convection zone, then $H_1(w)$ for any other pair of models can be written as

$$H_1(w) = \beta\phi(w) + H_s(w), \quad (11)$$

where $H_s(w)$ is a smooth component of $H_1(w)$ which results from sound-speed differences that arise from differences in the equation of state, abundances, surface physics etc., and the first term is the contribution to $H_1(w)$ due to the sound-speed difference caused by the difference in r_b , the position of the base of the CZ. Thus, if β is estimated using a least-squares fit, the unknown r_b of the Sun can be obtained. We determine β for a series of calibration models with different r_b , and interpolate to find the CZ position for which $\beta = 0$. This “null” method allows us to determine the position of the base of the CZ to a precision that is much better than what can be obtained with a sound-speed inversion, and is not hampered by the limited spatial resolution of inversions at the CZ base.

The uncertainty in our results arising from data uncertainties is evaluated by Monte Carlo simulations. For each observed data set, we create 4000 sets of artificial data by adding random realizations of the observed uncertainty to the central frequency and splitting coefficients. We determine R_{eff} and ΔR_{eff} for each of the simulated sets. The final parameters that we adopt is the mean of the distribution of results and the standard deviation is the uncertainty. We have found that the distribution is Gaussian and hence using the mean and standard deviation is adequate.

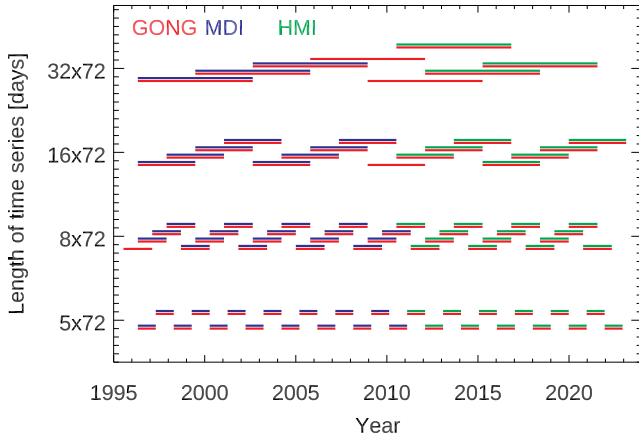


Figure 3. A visual representation of the time periods spanned by each SGK data set. Sets have been offset vertically for clarity. The sets, from top to bottom, are for 32×72 , 16×72 , 8×72 and 5×72 days respectively. Red denotes GONG, blue MDI and green HMI observations.

As is clear from the above discussion, we need to use models with a specified CZ depth. This can be done if we construct models of the solar envelope, for which the position of the CZ base and the helium abundance of the solar envelope can be specified.

Basu & Antia (1997) had shown that the largest source of systematic error in the estimated CZ-base position is the hydrogen abundance profile. This is because the sound speed near the base of the CZ is affected not only by the change in the temperature gradient but also by the change in the mean molecular weight due to gravitational settling of helium. This error does not affect this work since we are looking at differences with respect to the spherically symmetric component of the CZ base, and thus this ought to cancel out. Nevertheless, to minimize the error, we use models that have X and Z profiles for the Sun determined by Antia & Chitre (1998). However, since the position of the CZ base is well-known, we use calibration models with a smaller range in CZ positions — $0.7125R_{\odot}$, $0.7130R_{\odot}$, $0.7135R_{\odot}$, $0.7140R_{\odot}$, and $0.7145R_{\odot}$. We show in Fig. 2 how $H_1(w)$ changes when solar models with different CZ positions are used.

4. DATA USED

For this work, we use solar oscillation frequencies obtained by the ground-based Global Oscillation Network Group (GONG; Hill et al. 1996) and the space-based Michelson Doppler Imager (MDI) on board the Solar and Heliospheric Observatory spacecraft (Scherrer et al. 1995) and the Helioseismic and Magnetic Imager (HMI; Scherrer et al. 2012) on board the Solar Dynamics Observatory. We use mode frequencies obtained from different lengths of the time-series that cover solar cy-

cles 23 and 24. In particular, we use data analyzed by an alternative pipeline (Korzennik 2004, 2008a,b; Korzennik & Eff-Darwich 2013; Korzennik 2017, 2018, 2023), independent of the project’s pipeline, and henceforth referred to as the “SGK” pipeline. The mode parameters are derived from time-series that are multiples of 72 days, we use mode frequencies and splittings obtained for time-series lengths of $32 \times$, $16 \times$, $8 \times$ and 5×72 days, or $\simeq 6, 3, 1.5$ or 1 year, respectively. The choice of analyzing time series that are multiples of 72 days was dictated by the standard time-series length adopted by the MDI team, and was later adopted by the HMI team. A time-series of 72 days was considered to be long enough to produce a frequency spectrum with high signal-to-noise ratio but short enough to maintain “good” temporal variation, since the mode frequencies were known to vary with time on all time-scales. The MDI and HMI teams later started analyzing 360-day (i.e., 5×72 -day) long time series too.

Fig. 3 shows the temporal ranges the different data sets span. For time-series longer than 72 days, the convention adopted by SGK is to fit time-series separated by half the length of the time-series to increase the temporal resolution. The exception is for the 360-day long time-series, these are fitted every 360 day, to match what is done by the MDI project. Additionally, to determine the average asphericity over the two solar cycles, we used a GONG data set resulting from fitting a 128×72 -day time-series.

In some case, we also use mode parameters from the MDI and HMI projects’ pipeline. Although the primary frequency sets derived by these projects are obtained by fitting 72-day long time-series, which is not adequate for our work. However, there are some sets of frequencies and splittings obtained fitting 5×72 -day long time-series, and also one HMI set obtained from fitting a 32×72 -day long time-series.

It should be noted that the SGK pipeline predominantly obtains mode parameters by fitting asymmetric profiles to peaks in the power spectra, though some sets fitted using symmetric profiles are available. The MDI and HMI projects’ pipeline predominantly fits symmetric profiles, though some sets fitted using asymmetric profiles are available.

We restrict ourselves to modes with frequencies between 1.6 mHz and 3.5 mHz that have lower turning points between $0.45R_{\odot}$ and $0.95R_{\odot}$. These modes give good coverage of the CZ base, while keeping mode uncertainties low.

The SGK pipeline produces modes and splittings using a number of different leakage matrices. In one case, it uses the leakage matrix computed by the MDI/HMI

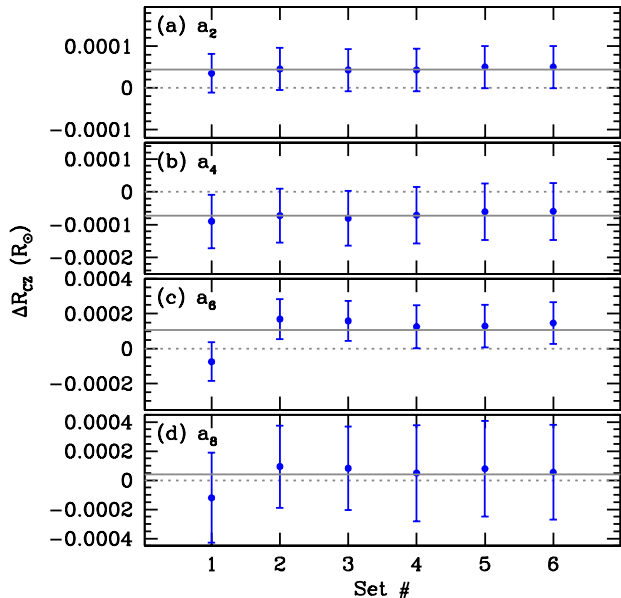


Figure 4. The figure shows the effect of the leakage matrix on ΔR_{CZ} implied by even-order splitting coefficients a_2 – a_8 (Panels (a), (b), (c) and (d) respectively) obtained for mode frequencies and splittings obtained with 32×72 -day time-series data from GONG and HMI with a start date of 2010:07:11 using different leakage matrices. The solid gray horizontal line in each panel is the weighted mean of all the results. The dotted gray line marks where results would lie if the CZ base were spherically symmetric. Set 1 is the HMI pipeline set, while set 2 is the SGK pipeline using GONG data and the JSBo=0 leakage matrix, set 3 is the SGK pipeline using GONG and the SKBo=0 leakage matrix, set 4 is the SGK pipeline using the HMI data and the JSBo=0 leakage matrix, set 5 is the SGK pipeline using HMI data and the SKBo=0 leakage matrix, and set 6 is the SGK pipeline using the HMI data and the SKBo=a2 leakage matrix.

project (JSBo=0), in the other cases it uses a leakage matrix computed by Korzennik (SKBo=0 & SKBo=a2). Such leakage matrix coefficients are computed as follows: a series of images of spherical harmonics on the unit sphere are computed, using the observational image projection, for either a heliographic latitude at disk center, B_o of 0, or 5.06° , the quadratic mean of B_o over a year. Each image is then spatially decomposed using the same decomposition procedure that is used for the respective observations. However, as can be seen in Fig. 4, the leakage matrix does not change the results to any level of statistical significance. The results in Fig. 4 are for 32×72 -day data sets with a start date of 2010:07:11. Unfortunately, MDI data does not exist for that time period. However, tests with MDI data for other spans of time give very similar results. Consequently, for all

subsequent results reported in this paper, we only use modes obtained with the JSBo=0 leakage matrix.

5. RESULTS

Our results derived from the 128×72 -day set are shown in Fig. 5. The values are tabulated in Table 1 in the Appendix. We find that the departure from sphericity, averaged over solar cycles 23 and 24 is extremely small, with only marginal statistical significance. When the contributions of the different components are combined to give the latitudinal difference, it is clear that we can at most give an upper limit of $0.0001 R_\odot$.

Earlier investigations, mentioned in Section 1 obtained much larger deviations. This could have been because of the quality of the then available data, or possibly because there is a time dependence to the asphericity, which is averaged out by the long, 128×72 -day, time-series. To test this, we used data sets obtained from shorter time-series. The resulting estimates of ΔR_{CZ} are shown in Fig. 6, and are tabulated in the Appendix.

A few features can be seen immediately. The scatter in the results obtained with the shorter time-series data is larger than those with the longer time-series data. This is, of course, expected given that the uncertainty in the mode frequencies and splittings is lower for the longer sets. The results obtained with GONG data agree with those of MDI and HMI data. The agreement is, however, better between GONG and HMI than between GONG and MDI. This type of disagreement has been seen in other helioseismic investigations, even when using the respective projects' pipeline data (e.g., Antia & Basu 2022).

We can also see that the scatter in the results do not appear to be strictly random. The right-hand panels of Fig. 7 give the impression of a possible anti-correlation between solar activity and CZ asphericity. Tests for such anti-correlation, where we used the 10.7cm radio flux averaged over the same time interval as an index of solar activity, do not reveal any statistically significant correlation. The largest anti-correlation is obtained for the a_4 results obtained with 32×72 -day time series, and even that is significant only at the $2\text{-}\sigma$ level. A strict solar cycle dependence is not really expected — the time variation of the tachocline is, after all, much more complicated with a clear sign of hysteresis (Basu & Antia 2019), hence there may still be a time variation just like in the tachocline. This seeming time variation is clearer for the results derived from the longer time-series, however, the variation becomes smaller as the length of the time-series is increased. This is to be expected if the time variation is real, since the longer sets would average out the time variations, but this can be merely a

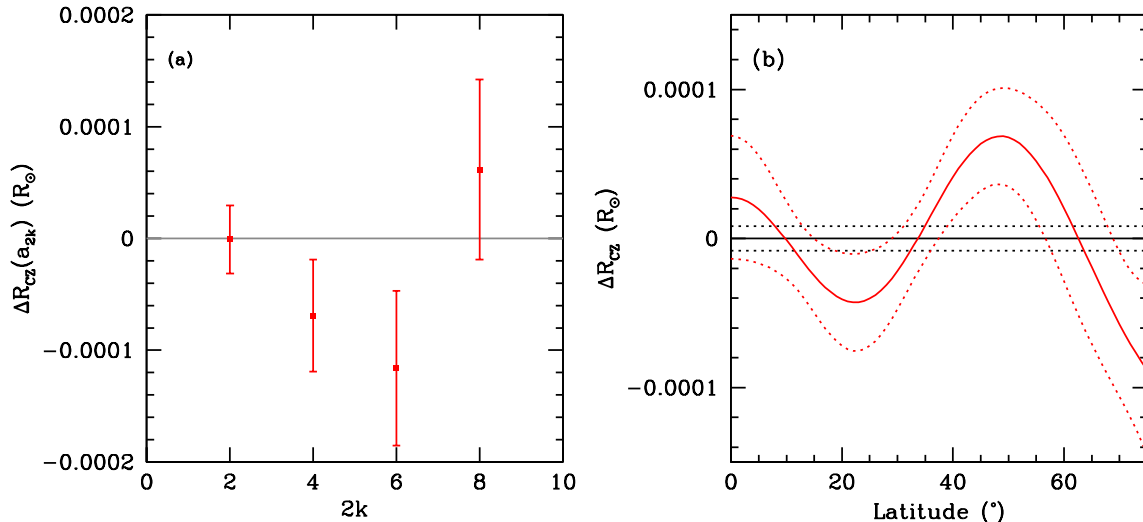


Figure 5. Left: Deviations from sphericity of the base of the CZ implied by different splitting coefficients a_{2k} for $2k = 1-4$. Right: The latitudinal variation of the asphericity implied by the results of the individual coefficients is shown as the red continuous line with the dotted line showing 1σ uncertainties. The black dotted lines show the 1σ uncertainty limit for the spherically symmetric component of the CZ base.

result of the observed uncertainties rather than a real temporal variation — as the uncertainties get reduced, the amplitude of the inferred variations will decrease.

We first verify whether the results obtained by the shorter time-series are consistent with those obtained with longer time-series. For this, we compare the results obtained with 16×72 -day data with those obtained with the average mode parameters of shorter sets — we averaged mode frequencies and splittings of $2 \times 8 \times 72$ -day sets and $3 \times 5 \times 72$ -day sets for each 16×72 -day set, we also averaged mode frequencies and splittings of $2 \times 16 \times 72$ -day sets for each 32×72 -day set. Note that $3 \times 5 \times 72$ -day sets do not quite cover a 16×72 -day set, but they are close enough. Also note that obtaining mode parameters from a long time-series is not the same as averaging mode parameters from shorter time-series because in the former case many more modes can rise above the noise level, while in the latter the set of successfully fitted modes is not always the same. The results are shown in Fig. 7. We also show results obtained by averaging frequencies and splittings of $2 \times 16 \times 72$ -day sets and compare those with the results of the 32×72 -day sets. As can be seen, averaging the mode parameters of the shorter sets yields results that are commensurate with those obtained with the longer sets.

Figs. 6 and 7 also shows that while a_2 , a_4 and, a_6 results show deviations from asphericity $> 1\sigma$ at some epochs, while the uncertainties in the a_8 results are too large to make any firm deduction about the contribution of a_8 to the asphericity of the CZ base.

5.1. Tests for time variations

The different panels in Figs. 6 suggest the possibility of a time variation; such putative variation is clearer in Fig. 7.

Given that the deviations from zero are small, we have performed additional tests to ascertain whether there really is a non-random variation.

We performed a Wald-Wolfowitz runs test (Wald & Wolfowitz 1940). While we tested the results from the GONG data sets separately, we combine the MDI and HMI sets. However, since our results have uncertainties, the results of one runs test is not adequate. Thus, for each data set (i.e., each length of time-series), we generated multiple sets by adding random realizations of the uncertainties to the results at each epoch. We also create a truly random set of results at each epoch; these are just random realizations of the uncertainties in the results. For each sequence of the realization of results and as well as the random set, we perform the runs test to derive a distribution of runs.

We compare the distribution of the runs test from our results and the random sequence. Note that since the uncertainties in the results at each epoch are very similar, the distribution of runs in our random case can be described by a Gaussian. We conduct the usual two-sample Kolmogorov-Smirnov test, as well as a Student's t test and an F test, to examine the null hypothesis that the distribution of runs in our results is drawn from the distribution of runs for the sample whose time variation is random. Because we are essentially dealing with small number statistics (in terms of the number of epochs covered, in other words the number of runs we can get), we relied on multiple measures of differences between the

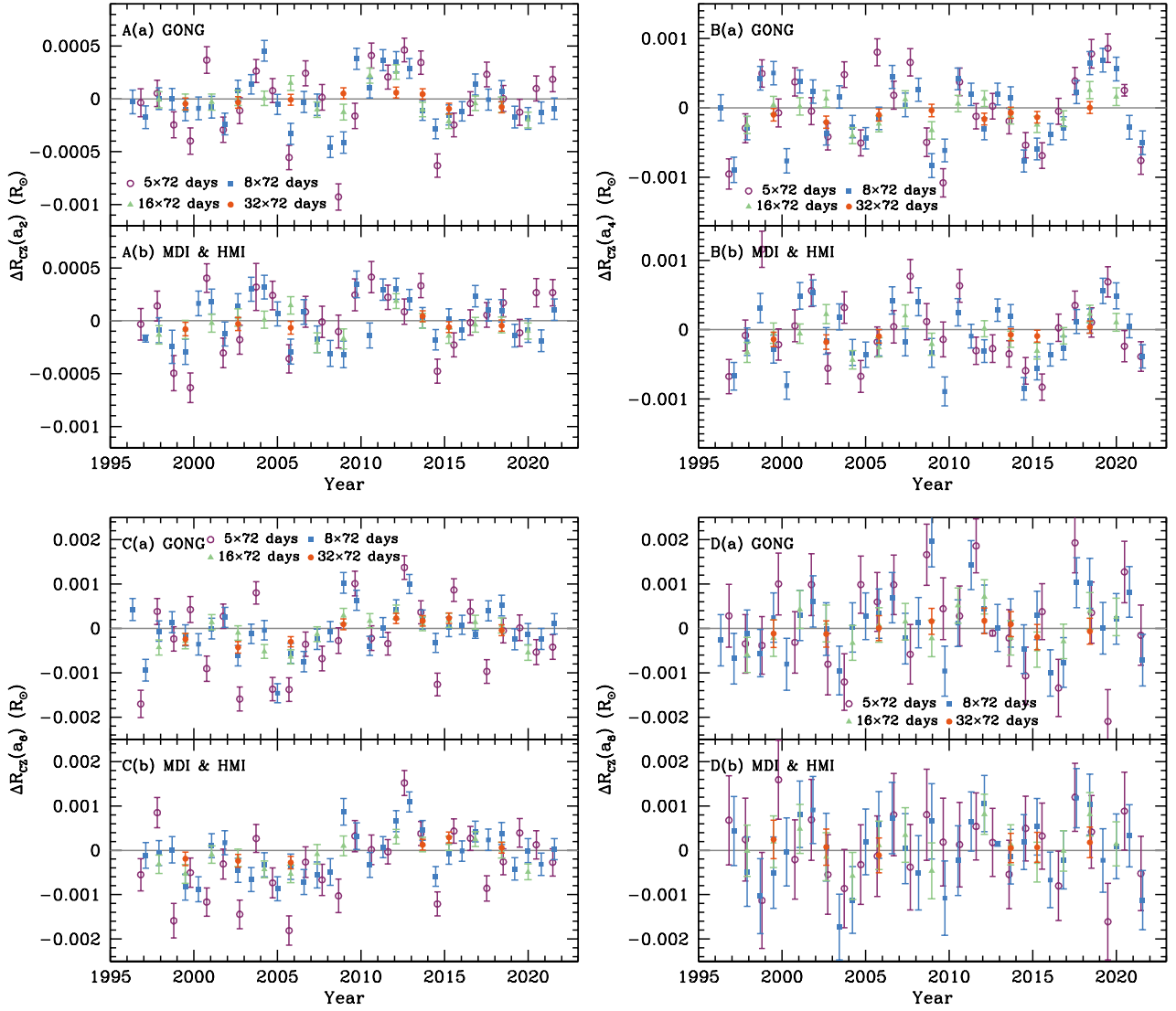


Figure 6. The deviation of the CZ base from spherical, ΔR_{CZ} , obtained with different lengths of time-series plotted as a function of time. Panels (A)–(D) are results for a_2 – a_8 respectively. Sub-panel (a) in all panels shows results with GONG data, while sub-panel (b) are for MDI and HMI data. Only results obtained with the SGK pipeline fitting asymmetric profiles are shown.

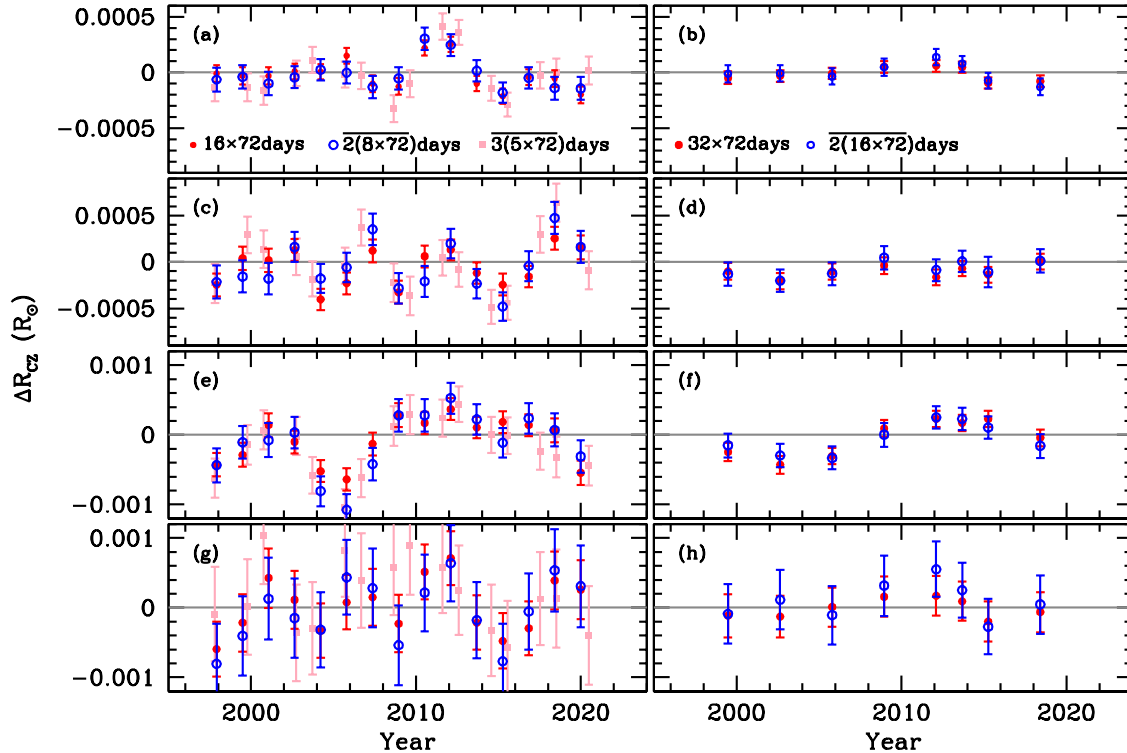


Figure 7. A comparison of our estimates of ΔR_{CZ} obtained with long time-series data and those with averaged mode parameters of shorter data. Only results obtained with GONG data are shown, since the data cover both solar cycle 23 and 24. The column on the left compares results from 16×72 -day time-series with those obtained with average mode parameters of 2 (8×72)-day sets and 3 (5×72)-day sets. The column on the right compares 32×72 -day results with those obtained from the average mode parameters of 2 (16×72)-day time-series. The rows from top to bottom show results for a_2 - a_8 respectively.

distributions of runs in the results and the distribution of runs in the random sample.

The statistical tests yield marginal evidence for a non-random time variation in most cases. The tests generally yield p values greater than 0.05 for a_2 and a_4 , however, for a_6 , we consistently get p values less than 0.05, and in some cases even more significant evidence of non-randomness. The combination of MDI and HMI results show the same pattern, though the significance is generally lower.

5.2. Examining possible sources of error

As shown above, the time-averaged signature of asphericity is very small, evidence of time-variation is also marginal. To ensure that our results are robust, we take a close look at possible sources of error that could cause a spurious time dependence in our results.

5.2.1. The second-order effects of rotation

The even-order a coefficients have a small contribution from the second-order effects of rotation (Gough & Thompson 1990). It is known that solar rotation changes with time (see e.g., Antia & Basu 2013; Howe et al. 2013; Komm et al. 2018; Howe et al.

2018; Kosovichev & Pipin 2019; Antia & Basu 2022, etc.), even near the base of the solar convection zone (Basu & Antia 2019), the region of interest for this work. We did not correct the data for the second-order effect of rotation. In order to examine the effect of the second-order effects, we remove those from the GONG 16×72 -day data-sets; we do so using the formalism of Antia et al. (2000) and determine the asphericity again.

The differences between the uncorrected and corrected results, normalized by the uncertainty in the corrected result, are shown in Fig. 8. As can be seen, while the differences are systematic, they are a small fraction of the uncertainty. The difference is largest for $\Delta R_{CZ}(a_2)$, but even there, the differences are less than 0.5σ . Furthermore, although rotation is time-dependent, that does not affect the asphericity results.

5.2.2. The surface term

The surface term is the frequency-dependent frequency offset between the Sun and a solar model. This offset increases with frequency. It is well known that the solar surface term changes with solar cycle (Elsworth et al. 1990; Libbrecht & Woodard 1990; Howe et al. 2017, etc.), being largest at solar maximum

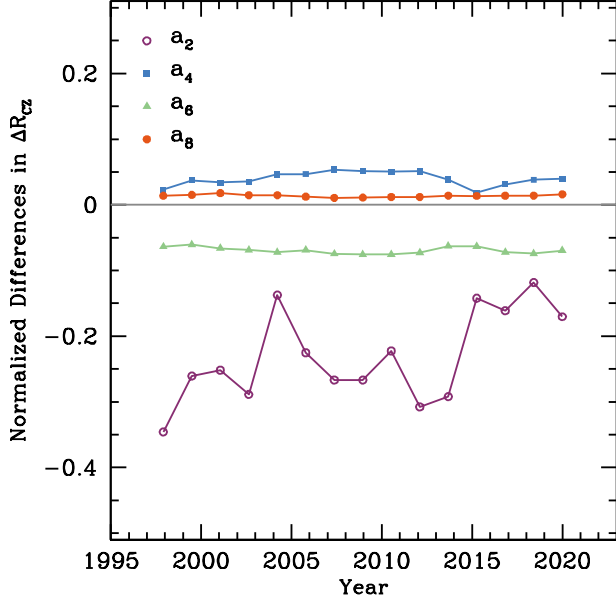


Figure 8. The difference in the original estimates of asphericity and those estimated using data sets corrected for the second order effects of rotation, normalized by the uncertainties in the original result. These results were obtained with GONG 16×72 -day data sets.

and smallest at the minimum. The surface term has a steep frequency difference, and hence, to examine whether we remove it completely through Eq. 10, we re-determine ΔR_{CZ} after reducing the upper frequency limit from 3.5 to 3 mHz. The results are shown in Fig. 9. As can be seen, differences between results with different upper frequency cut-off are generally well within 1σ . These differences do not show a solar cycle dependence, something we would expect to see had we not removed the surface term.

5.3. Asymmetry of the mode profiles

As mentioned earlier, the data sets that we use determined frequencies and splittings by fitting an asymmetric profile to the peaks in the oscillation power spectra. In order to discount asymmetry as the source of time variation, we compared the 5×72 -day results obtained when fitting using either symmetric or asymmetric mode profiles. The differences, normalized by the uncertainty, are shown in Fig. 10. As can be seen, the differences are generally within 1σ and the time variations do not look anything like the ones seen in Figs. 6 and 7.

The MDI and HMI project pipelines also produce data sets from 5×72 -day time-series mainly by fitting symmetric profiles, but some sets have also been fit using asymmetric profile. This allows us to compare results

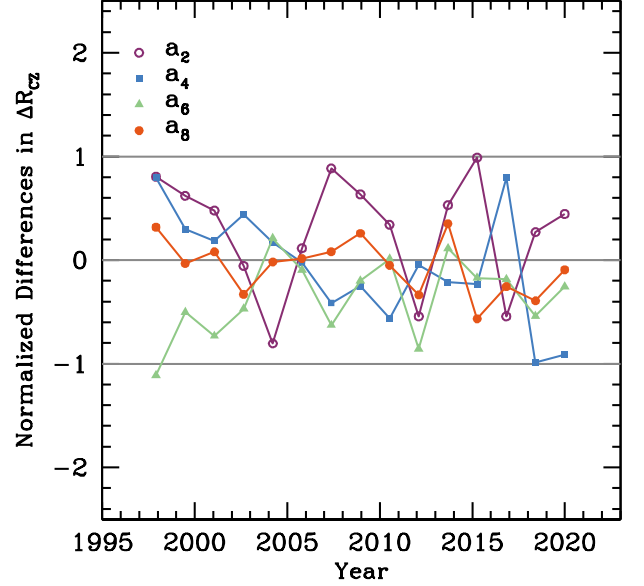


Figure 9. The change in ΔR_{CZ} estimates, when the splittings were restricted to modes with frequencies ≤ 3 mHz, normalized by their uncertainty, obtained when using 16×72 -day GONG data sets. The horizontal lines mark 0 and $\pm 1\sigma$ differences. Note that most results are well within 1σ and that there is no solar-cycle dependence.

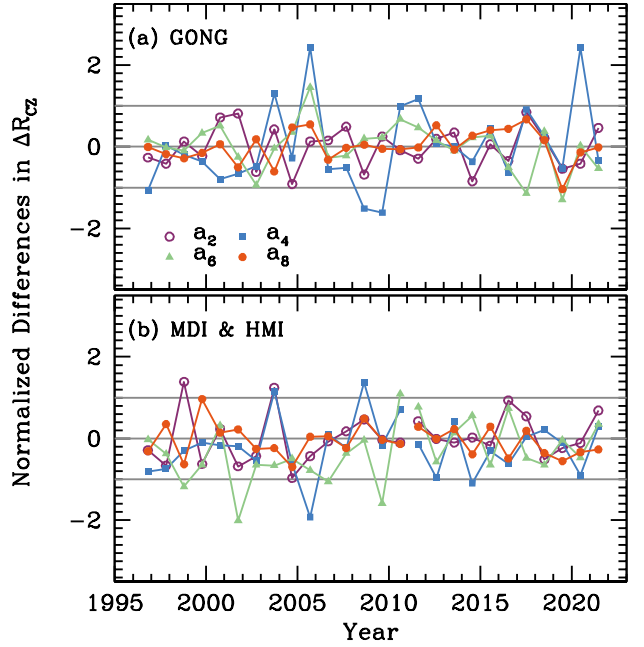


Figure 10. The difference in ΔR_{CZ} estimates, normalized by uncertainty, obtained with mode parameters asymmetric and symmetric fits to the data from the SGK pipeline for the 5×72 -day time-series. The horizontal lines mark 0 and $\pm 1\sigma$ differences.

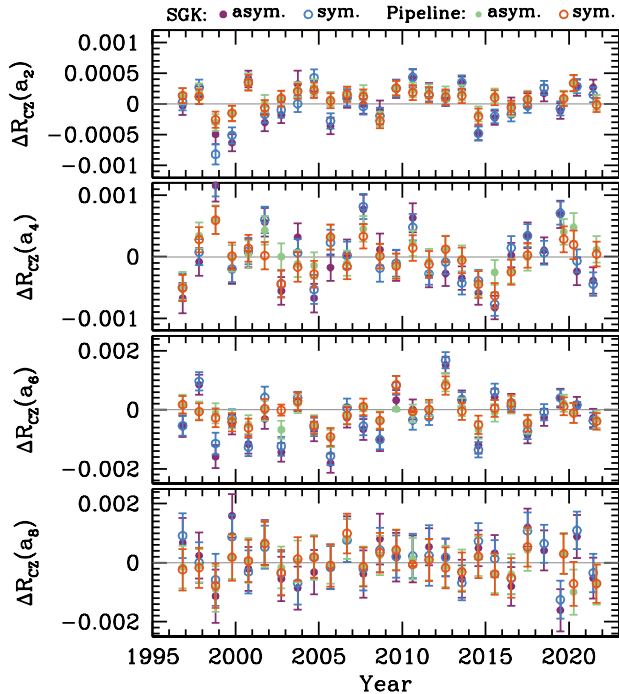


Figure 11. Asphericity parameter ΔR_{CZ} obtained with 5×72 -day MDI and HMI project pipeline data as well as with SGK pipeline data fitted using both symmetric and asymmetric peak profiles. The rows from top to bottom are for a_2 – a_8 respectively. While Fig. 10 shows the normalized difference between two sets, this figure shows the actual values for four sets of data.

obtained with the project pipeline data with the SGK pipeline data, as shown in Fig. 11.

6. DISCUSSION AND CONCLUSIONS

We have used global helioseismic data, frequencies and a_2 – a_8 even-order splitting coefficients, available from various sources and derived using different methodologies as well as time-series of various lengths, all collected over solar cycles 23 and 24, to determine whether the base of the solar convection zone is aspherical.

Using a data set obtained from a 128×72 -day time-series, we find that the time-averaged asphericity of the CZ base is small, with an upper limit of $0.0001R_\odot$ on the deviation from sphericity.

Our new estimate is smaller than those derived by earlier work. There are a number of reasons this could be the case. For one, all previous estimates used data sets from much shorter time-series, which means larger uncertainties that results in a larger uncertainty on the amplitude. Alternatively, if there is indeed a small variation, using a shorter time-series could make it more visible. And yet another possible reason for the discrepancy is the method by which asphericity is determined.

Our results are much smaller than the estimates of Gough & Kosovichev (1995). It is possible that the Gough & Kosovichev (1995) inversion results (for the isothermal sound speed u with the helium abundance Y as the second parameter) have errors because calculating (u, Y) kernels requires one to assume that the equation of state of solar material is known and is the same as that of the reference model; Basu & Christensen-Dalsgaard (1997) have shown that this leads to systematic errors in the inversion results both above and below the CZ base and also results in unrealistically small uncertainties.

It is more difficult to compare our results with those of Monteiro et al. (2001) since they do not translate their acoustic depth differences into differences in radius. An acoustic depth difference of 100 seconds at the CZ base translates to a radius difference of approximately $0.025 R_\odot$, again much larger than what we find. One of the possible reasons for this is that Monteiro et al. (2001) only fit the acoustic glitch at the CZ base and neglect the contribution from the helium ionization zone, and additionally do not take the surface-term into account. The glitch signature from the helium ionization zone is known to vary with solar cycle (Basu & Mandel 2004; Watson & Basu 2020), and the surface term is not only time dependent, the time-dependence depends on latitude (Antia et al. 2001b; Basu et al. 2007). Not taking the latitudinal dependence of the surface term into account could lead to a large asphericity, while the time-varying signature from the helium ionization zone could add to the time-dependence of their results. Our results are smaller than, but in line with, those of Basu & Antia (2001). Basu & Antia (2001) used shorter time-series data and averaged the results over slightly more than four years, but that is still a much shorter time interval than 25-years, which is what we use for our main results.

We have tested our results to examine whether there is a non-random time dependence in the results. Only the a_6 component gives a p -value of less than 0.05. Our efforts to determine whether there is a real time-dependence are hampered by the small number of data sets we have. Results obtained with data from short time-series (like the usual 72-day sets from the project pipelines) have unfortunately very large uncertainties, but increasing the length of the time-series decreases the number of sets covering the two solar cycles, and additionally average out any underlying time dependence.

Determining the cause of the asphericity, and any possible changes thereof, is beyond the scope of the paper. However, assuming that the asphericity is an indirect result of magnetic fields and the resulting modification of the thermal structure, a shift in the CZ

base of $0.0001R_{\odot}$ implies a magnetic field of ~ 300 kG. This is consistent with the limits on the magnetic fields at the base of the CZ of a few hundred kilo-Gauss (e.g., D’Silva & Choudhuri 1993; Basu 1997; Antia et al. 2000, 2003).

ACKNOWLEDGEMENTS

We thank H. M. Antia for his comments on an earlier draft of the paper that led us to conduct statistical tests to ascertain the significance of the temporal variations and for his help in calculating the second-order effects of rotation. This work is supported by NASA grant 80NSSC23K0563 to SB and NASA grants 80NSSC22K0516 and NNH18ZDA001N-DRIVE to SGK. This work utilizes data from the National Solar Observatory Integrated Synoptic Program, which is operated by the Association of Universities for Re-

search in Astronomy, under a cooperative agreement with the National Science Foundation and with additional financial support from the National Oceanic and Atmospheric Administration, the National Aeronautics and Space Administration, and the United States Air Force. The GONG network of instruments is hosted by the Big Bear Solar Observatory, High Altitude Observatory, Learmonth Solar Observatory, Udaipur Solar Observatory, Instituto de Astrofísica de Canarias, and Cerro Tololo Interamerican Observatory. This work also uses provided by the SOHO/MDI consortium. SOHO is a project of international cooperation between ESA and NASA. We also use data from the Helioseismic and Magnetic Imager on board the Solar Dynamics Observatory. HMI data are courtesy of NASA/SDO and the AIA, EVE, and HMI science teams.

REFERENCES

- Antia, H. M., & Basu, S. 1994, *A&AS*, 107, 421
- Antia, H. M., & Basu, S. 2013, in *Journal of Physics Conference Series*, Vol. 440, *Journal of Physics Conference Series*, 012018, doi: [10.1088/1742-6596/440/1/012018](https://doi.org/10.1088/1742-6596/440/1/012018)
- . 2022, *ApJ*, 924, 19, doi: [10.3847/1538-4357/ac32c3](https://doi.org/10.3847/1538-4357/ac32c3)
- Antia, H. M., Basu, S., & Chitre, S. M. 1998, *MNRAS*, 298, 543, doi: [10.1046/j.1365-8711.1998.01635.x](https://doi.org/10.1046/j.1365-8711.1998.01635.x)
- Antia, H. M., Basu, S., Hill, F., et al. 2001a, *MNRAS*, 327, 1029, doi: [10.1046/j.1365-8711.2001.04819.x](https://doi.org/10.1046/j.1365-8711.2001.04819.x)
- . 2001b, *MNRAS*, 327, 1029, doi: [10.1046/j.1365-8711.2001.04819.x](https://doi.org/10.1046/j.1365-8711.2001.04819.x)
- Antia, H. M., & Chitre, S. M. 1998, *A&A*, 339, 239
- Antia, H. M., Chitre, S. M., & Thompson, M. J. 2000, *A&A*, 360, 335, doi: [10.48550/arXiv.astro-ph/0005587](https://doi.org/10.48550/arXiv.astro-ph/0005587)
- . 2003, *A&A*, 399, 329, doi: [10.1051/0004-6361:20021760](https://doi.org/10.1051/0004-6361:20021760)
- Basu, S. 1997, *MNRAS*, 288, 572, doi: [10.1093/mnras/288.3.572](https://doi.org/10.1093/mnras/288.3.572)
- . 1998, *MNRAS*, 298, 719, doi: [10.1046/j.1365-8711.1998.01690.x](https://doi.org/10.1046/j.1365-8711.1998.01690.x)
- Basu, S., & Antia, H. M. 1997, *MNRAS*, 287, 189, doi: [10.1093/mnras/287.1.189](https://doi.org/10.1093/mnras/287.1.189)
- . 2001, *MNRAS*, 324, 498, doi: [10.1046/j.1365-8711.2001.04364.x](https://doi.org/10.1046/j.1365-8711.2001.04364.x)
- . 2019, *ApJ*, 883, 93, doi: [10.3847/1538-4357/ab3b57](https://doi.org/10.3847/1538-4357/ab3b57)
- Basu, S., Antia, H. M., & Bogart, R. S. 2007, *ApJ*, 654, 1146, doi: [10.1086/509251](https://doi.org/10.1086/509251)
- Basu, S., & Christensen-Dalsgaard, J. 1997, *A&A*, 322, L5, doi: [10.48550/arXiv.astro-ph/9702162](https://doi.org/10.48550/arXiv.astro-ph/9702162)
- Basu, S., & Mandel, A. 2004, *ApJL*, 617, L155, doi: [10.1086/427435](https://doi.org/10.1086/427435)
- Charbonneau, P., Christensen-Dalsgaard, J., Henning, R., et al. 1999, *ApJ*, 527, 445, doi: [10.1086/308050](https://doi.org/10.1086/308050)
- Christensen-Dalsgaard, J., Gough, D. O., & Thompson, M. J. 1991, *ApJ*, 378, 413, doi: [10.1086/170441](https://doi.org/10.1086/170441)
- Christensen-Dalsgaard, J., Proffitt, C. R., & Thompson, M. J. 1993, *ApJL*, 403, L75, doi: [10.1086/186725](https://doi.org/10.1086/186725)
- Christensen-Dalsgaard, J., Thompson, M. J., & Gough, D. O. 1989, *MNRAS*, 238, 481, doi: [10.1093/mnras/238.2.481](https://doi.org/10.1093/mnras/238.2.481)
- D’Silva, S., & Choudhuri, A. R. 1993, *A&A*, 272, 621
- Elsworth, Y., Howe, R., Isaak, G. R., McLeod, C. P., & New, R. 1990, *Nature*, 345, 322, doi: [10.1038/345322a0](https://doi.org/10.1038/345322a0)
- Gough, D. O., & Kosovichev, A. G. 1995, in *ESA Special Publication*, Vol. 376, *Helioseismology*, ed. J. T. Hoeksema, V. Domingo, B. Fleck, & B. Battrick, 47
- Gough, D. O., & Thompson, M. J. 1990, *MNRAS*, 242, 25, doi: [10.1093/mnras/242.1.25](https://doi.org/10.1093/mnras/242.1.25)
- Hill, F., Stark, P. B., Stebbins, R. T., et al. 1996, *Science*, 272, 1292
- Howe, R., Basu, S., Davies, G. R., et al. 2017, *MNRAS*, 464, 4777, doi: [10.1093/mnras/stw2668](https://doi.org/10.1093/mnras/stw2668)
- Howe, R., Christensen-Dalsgaard, J., Hill, F., et al. 2013, in *Astronomical Society of the Pacific Conference Series*, Vol. 478, *Fifty Years of Seismology of the Sun and Stars*, ed. K. Jain, S. C. Tripathy, F. Hill, J. W. Leibacher, & A. A. Pevtsov, 303
- Howe, R., Hill, F., Komm, R., et al. 2018, *ApJL*, 862, L5, doi: [10.3847/2041-8213/aad1ed](https://doi.org/10.3847/2041-8213/aad1ed)
- Komm, R., Howe, R., & Hill, F. 2018, *SoPh*, 293, 145, doi: [10.1007/s11207-018-1365-7](https://doi.org/10.1007/s11207-018-1365-7)

- Korzennik, S. G. 2004, in ESA Special Publication, Vol. 559, SOHO 14 Helio- and Asteroseismology: Towards a Golden Future, ed. D. Danesy, 524.
<https://arxiv.org/abs/astro-ph/0406470>
- Korzennik, S. G. 2008a, *Astronomische Nachrichten*, 329, 453, doi: [10.1002/asna.200710979](https://doi.org/10.1002/asna.200710979)
- Korzennik, S. G. 2008b, in Journal of Physics Conference Series, Vol. 118, Journal of Physics Conference Series, 012082, doi: [10.1088/1742-6596/118/1/012082](https://doi.org/10.1088/1742-6596/118/1/012082)
- Korzennik, S. G. 2017, in AAS/Solar Physics Division Meeting, Vol. 48, AAS/Solar Physics Division Abstracts #48, 113.02
- Korzennik, S. G. 2018, in Catalyzing Solar Connections, 132 —. 2023, *Frontiers in Astronomy and Space Sciences*, 9, 1031313, doi: [10.3389/fspas.2022.1031313](https://doi.org/10.3389/fspas.2022.1031313)
- Korzennik, S. G., & Eff-Darwich, A. 2013, in Journal of Physics Conference Series, Vol. 440, Journal of Physics Conference Series, 012015, doi: [10.1088/1742-6596/440/1/012015](https://doi.org/10.1088/1742-6596/440/1/012015)
- Kosovichev, A. G. 1999, *Journal of Computational and Applied Mathematics*, 109, 1
- Kosovichev, A. G., & Pipin, V. V. 2019, *ApJL*, 871, L20, doi: [10.3847/2041-8213/aaf82](https://doi.org/10.3847/2041-8213/aaf82)
- Kuhn, J. R., Bush, R., Emilio, M., & Scholl, I. F. 2012, *Science*, 337, 1638, doi: [10.1126/science.1223231](https://doi.org/10.1126/science.1223231)
- Libbrecht, K. G., & Woodard, M. F. 1990, *Nature*, 345, 779, doi: [10.1038/345779a0](https://doi.org/10.1038/345779a0)
- Monteiro, M. J. P. F. G., Christensen-Dalsgaard, J., Schou, J., & Thompson, M. J. 2001, in ESA Special Publication, Vol. 464, SOHO 10/GONG 2000 Workshop: Helio- and Asteroseismology at the Dawn of the Millennium, ed. A. Wilson & P. L. Pallé, 535–538
- Scherrer, P. H., Bogart, R. S., Bush, R. I., et al. 1995, *SoPh*, 162, 129
- Scherrer, P. H., Schou, J., Bush, R. I., et al. 2012, *SoPh*, 275, 207
- Schou, J., Howe, R., Basu, S., et al. 2002, *ApJ*, 567, 1234, doi: [10.1086/338665](https://doi.org/10.1086/338665)
- Spiegel, E. A., & Zahn, J. P. 1992, *A&A*, 265, 106
- Wald, A., & Wolfowitz, J. 1940, *Ann. Math. Statist.*, 11, 147, doi: [10.1214/aoms/1177731909](https://doi.org/10.1214/aoms/1177731909)
- Watson, C. B., & Basu, S. 2020, *ApJL*, 903, L29, doi: [10.3847/2041-8213/abc348](https://doi.org/10.3847/2041-8213/abc348)
- Woodard, M. F., & Libbrecht, K. G. 1993, *ApJL*, 402, L77, doi: [10.1086/186704](https://doi.org/10.1086/186704)
- Zweibel, E. G., & Gough, D. 1995, in ESA Special Publication, Vol. 376, Helioseismology, ed. J. T. Hoeksema, V. Domingo, B. Fleck, & B. Battrick, 73

APPENDIX

We tabulate our results for the SGK asymmetric sets in Tables 1, 2, 3, 4 and 5. Note that the start date of each set is in YYYYMMDD format.

Table 1. Results for the 128×72 -day set

Start Date of set	$\Delta R_{CZ}/R_{\odot}$			
	a_2	a_4	a_6	a_8
19960501	$-9.4590\text{E}-07 \pm 3.032\text{E}-05$	$-6.913\text{E}-05 \pm 5.007\text{E}-05$	$-1.159\text{E}-04 \pm 6.921\text{E}-05$	$6.173\text{E}-05 \pm 8.067\text{E}-05$

Table 2. Results for the 32×72 -day sets

Start Date of set	$\Delta R_{CZ}/R_{\odot}$			
	a_2	a_4	a_6	a_8
GONG				
19960501	$-4.738\text{E}-05 \pm 5.718\text{E}-05$	$-1.002\text{E}-04 \pm 9.185\text{E}-05$	$-2.444\text{E}-04 \pm 1.333\text{E}-04$	$-1.163\text{E}-04 \pm 3.116\text{E}-04$
19990627	$-3.263\text{E}-05 \pm 5.430\text{E}-05$	$-2.082\text{E}-04 \pm 8.657\text{E}-05$	$-4.283\text{E}-04 \pm 1.279\text{E}-04$	$-1.265\text{E}-04 \pm 2.975\text{E}-04$
20020822	$-8.575\text{E}-06 \pm 5.061\text{E}-05$	$-1.016\text{E}-04 \pm 8.703\text{E}-05$	$-3.006\text{E}-04 \pm 1.172\text{E}-04$	$8.281\text{E}-06 \pm 2.824\text{E}-04$
20051017	$5.070\text{E}-05 \pm 5.268\text{E}-05$	$-3.764\text{E}-05 \pm 9.057\text{E}-05$	$9.180\text{E}-05 \pm 1.219\text{E}-04$	$1.601\text{E}-04 \pm 2.911\text{E}-04$
20081212	$5.876\text{E}-05 \pm 5.171\text{E}-05$	$-1.637\text{E}-04 \pm 8.471\text{E}-05$	$2.272\text{E}-04 \pm 1.165\text{E}-04$	$1.718\text{E}-04 \pm 2.881\text{E}-04$
20100711	$4.541\text{E}-05 \pm 5.081\text{E}-05$	$-7.202\text{E}-05 \pm 8.235\text{E}-05$	$1.693\text{E}-04 \pm 1.152\text{E}-04$	$9.342\text{E}-05 \pm 2.830\text{E}-04$
20120207	$-9.347\text{E}-05 \pm 5.085\text{E}-05$	$-1.363\text{E}-04 \pm 8.488\text{E}-05$	$2.298\text{E}-04 \pm 1.161\text{E}-04$	$-1.971\text{E}-04 \pm 2.869\text{E}-04$
20150404	$-7.865\text{E}-05 \pm 5.255\text{E}-05$	$3.237\text{E}-06 \pm 8.627\text{E}-05$	$-4.353\text{E}-05 \pm 1.204\text{E}-04$	$-6.526\text{E}-05 \pm 2.908\text{E}-04$
MDI				
19960501	$-7.867\text{E}-05 \pm 6.447\text{E}-05$	$-1.385\text{E}-04 \pm 1.051\text{E}-04$	$-1.907\text{E}-04 \pm 1.518\text{E}-04$	$2.438\text{E}-04 \pm 4.312\text{E}-04$
19990627	$-2.981\text{E}-05 \pm 6.308\text{E}-05$	$-1.783\text{E}-04 \pm 1.025\text{E}-04$	$-2.384\text{E}-04 \pm 1.443\text{E}-04$	$7.186\text{E}-05 \pm 4.077\text{E}-04$
20020822	$-6.684\text{E}-05 \pm 6.030\text{E}-05$	$-9.508\text{E}-05 \pm 9.902\text{E}-05$	$-2.753\text{E}-04 \pm 1.419\text{E}-04$	$-1.137\text{E}-04 \pm 3.954\text{E}-04$
HMI				
20100711	$4.329\text{E}-05 \pm 5.089\text{E}-05$	$-7.144\text{E}-05 \pm 8.622\text{E}-05$	$1.255\text{E}-04 \pm 1.221\text{E}-04$	$4.889\text{E}-05 \pm 3.299\text{E}-04$
20120207	$-5.962\text{E}-05 \pm 5.164\text{E}-05$	$-9.135\text{E}-05 \pm 8.593\text{E}-05$	$2.892\text{E}-04 \pm 1.213\text{E}-04$	$6.755\text{E}-05 \pm 3.368\text{E}-04$
20150404	$-4.604\text{E}-05 \pm 5.262\text{E}-05$	$3.790\text{E}-05 \pm 8.924\text{E}-05$	$5.797\text{E}-05 \pm 1.240\text{E}-04$	$1.780\text{E}-04 \pm 3.445\text{E}-04$

Table 3. Results for the 16×72 -day sets

Start Date of set	$\Delta R_{Cz}/R_{\odot}$			
	a_2	a_4	a_6	a_8
GONG				
19960501	$-9.578\text{E}-06 \pm 7.559\text{E}-05$	$-2.472\text{E}-04 \pm 1.247\text{E}-04$	$-4.292\text{E}-04 \pm 1.695\text{E}-04$	$-5.980\text{E}-04 \pm 3.937\text{E}-04$
19971128	$-3.080\text{E}-05 \pm 7.665\text{E}-05$	$4.067\text{E}-05 \pm 1.254\text{E}-04$	$-2.863\text{E}-04 \pm 1.721\text{E}-04$	$-2.182\text{E}-04 \pm 4.119\text{E}-04$
19990627	$-3.039\text{E}-05 \pm 7.607\text{E}-05$	$1.888\text{E}-05 \pm 1.256\text{E}-04$	$1.395\text{E}-04 \pm 1.717\text{E}-04$	$4.238\text{E}-04 \pm 4.263\text{E}-04$
20010123	$8.732\text{E}-06 \pm 7.203\text{E}-05$	$1.294\text{E}-04 \pm 1.196\text{E}-04$	$-1.026\text{E}-04 \pm 1.630\text{E}-04$	$1.114\text{E}-04 \pm 4.160\text{E}-04$
20020822	$4.753\text{E}-06 \pm 6.905\text{E}-05$	$-4.011\text{E}-04 \pm 1.150\text{E}-04$	$-5.198\text{E}-04 \pm 1.572\text{E}-04$	$-3.296\text{E}-04 \pm 3.920\text{E}-04$
20040320	$1.501\text{E}-04 \pm 7.010\text{E}-05$	$-2.298\text{E}-04 \pm 1.168\text{E}-04$	$-6.399\text{E}-04 \pm 1.588\text{E}-04$	$7.852\text{E}-05 \pm 3.892\text{E}-04$
20051017	$-1.015\text{E}-04 \pm 7.376\text{E}-05$	$1.206\text{E}-04 \pm 1.230\text{E}-04$	$-1.313\text{E}-04 \pm 1.660\text{E}-04$	$1.512\text{E}-04 \pm 4.082\text{E}-04$
20070516	$-1.252\text{E}-04 \pm 7.478\text{E}-05$	$-3.250\text{E}-04 \pm 1.248\text{E}-04$	$2.841\text{E}-04 \pm 1.684\text{E}-04$	$-2.288\text{E}-04 \pm 4.118\text{E}-04$
20081212	$2.202\text{E}-04 \pm 7.036\text{E}-05$	$6.091\text{E}-05 \pm 1.172\text{E}-04$	$1.707\text{E}-04 \pm 1.603\text{E}-04$	$5.158\text{E}-04 \pm 3.947\text{E}-04$
20100711	$2.534\text{E}-04 \pm 6.866\text{E}-05$	$1.315\text{E}-04 \pm 1.133\text{E}-04$	$3.695\text{E}-04 \pm 1.567\text{E}-04$	$7.099\text{E}-04 \pm 3.859\text{E}-04$
20120207	$-1.009\text{E}-04 \pm 6.826\text{E}-05$	$-1.183\text{E}-04 \pm 1.133\text{E}-04$	$1.037\text{E}-04 \pm 1.557\text{E}-04$	$-2.133\text{E}-04 \pm 3.893\text{E}-04$
20130905	$-2.129\text{E}-04 \pm 6.937\text{E}-05$	$-2.424\text{E}-04 \pm 1.162\text{E}-04$	$1.825\text{E}-04 \pm 1.587\text{E}-04$	$-4.772\text{E}-04 \pm 3.979\text{E}-04$
20150404	$-4.178\text{E}-05 \pm 6.884\text{E}-05$	$-1.570\text{E}-04 \pm 1.153\text{E}-04$	$1.379\text{E}-04 \pm 1.571\text{E}-04$	$-2.948\text{E}-04 \pm 3.890\text{E}-04$
20161031	$-5.547\text{E}-05 \pm 7.416\text{E}-05$	$2.548\text{E}-04 \pm 1.240\text{E}-04$	$6.474\text{E}-05 \pm 1.689\text{E}-04$	$3.919\text{E}-04 \pm 4.142\text{E}-04$
20180530	$-1.997\text{E}-04 \pm 7.548\text{E}-05$	$1.588\text{E}-04 \pm 1.278\text{E}-04$	$-5.430\text{E}-04 \pm 1.733\text{E}-04$	$2.581\text{E}-04 \pm 4.238\text{E}-04$
MDI				
19960501	$-1.333\text{E}-04 \pm 8.700\text{E}-05$	$-3.274\text{E}-04 \pm 1.439\text{E}-04$	$-3.134\text{E}-04 \pm 2.064\text{E}-04$	$-1.311\text{E}-05 \pm 5.777\text{E}-04$
19971128	$-8.289\text{E}-05 \pm 8.848\text{E}-05$	$-5.004\text{E}-05 \pm 1.460\text{E}-04$	$-5.322\text{E}-04 \pm 2.104\text{E}-04$	$1.935\text{E}-04 \pm 5.817\text{E}-04$
19990627	$-2.209\text{E}-05 \pm 8.436\text{E}-05$	$-5.543\text{E}-05 \pm 1.396\text{E}-04$	$-9.628\text{E}-05 \pm 1.983\text{E}-04$	$4.837\text{E}-04 \pm 5.509\text{E}-04$
20010123	$3.061\text{E}-05 \pm 8.254\text{E}-05$	$2.247\text{E}-04 \pm 1.365\text{E}-04$	$-1.705\text{E}-04 \pm 1.933\text{E}-04$	$-1.451\text{E}-04 \pm 5.396\text{E}-04$
20020822	$9.667\text{E}-06 \pm 8.087\text{E}-05$	$-4.345\text{E}-04 \pm 1.344\text{E}-04$	$-4.311\text{E}-04 \pm 1.901\text{E}-04$	$-5.783\text{E}-04 \pm 5.295\text{E}-04$
20040320	$1.466\text{E}-04 \pm 8.305\text{E}-05$	$-2.539\text{E}-04 \pm 1.373\text{E}-04$	$-5.356\text{E}-04 \pm 1.957\text{E}-04$	$1.133\text{E}-04 \pm 5.460\text{E}-04$
20051017	$-2.067\text{E}-04 \pm 9.270\text{E}-05$	$2.023\text{E}-04 \pm 1.536\text{E}-04$	$-8.969\text{E}-05 \pm 2.179\text{E}-04$	$3.453\text{E}-04 \pm 6.127\text{E}-04$
20070516	$-1.721\text{E}-04 \pm 9.550\text{E}-05$	$-2.101\text{E}-04 \pm 1.586\text{E}-04$	$1.006\text{E}-04 \pm 2.252\text{E}-04$	$-4.621\text{E}-04 \pm 6.324\text{E}-04$
HMI				
20100711	$1.855\text{E}-04 \pm 6.960\text{E}-05$	$1.310\text{E}-05 \pm 1.160\text{E}-04$	$3.097\text{E}-04 \pm 1.631\text{E}-04$	$8.094\text{E}-04 \pm 4.522\text{E}-04$
20120207	$8.665\text{E}-07 \pm 7.001\text{E}-05$	$-1.380\text{E}-04 \pm 1.169\text{E}-04$	$1.291\text{E}-04 \pm 1.629\text{E}-04$	$1.249\text{E}-04 \pm 4.519\text{E}-04$
20130905	$-1.444\text{E}-04 \pm 6.895\text{E}-05$	$-3.080\text{E}-04 \pm 1.159\text{E}-04$	$1.568\text{E}-04 \pm 1.612\text{E}-04$	$-2.675\text{E}-04 \pm 4.466\text{E}-04$
20150404	$-3.823\text{E}-05 \pm 6.993\text{E}-05$	$-8.838\text{E}-05 \pm 1.177\text{E}-04$	$2.527\text{E}-04 \pm 1.646\text{E}-04$	$-1.293\text{E}-05 \pm 4.568\text{E}-04$
20161031	$-3.855\text{E}-05 \pm 7.470\text{E}-05$	$2.291\text{E}-04 \pm 1.261\text{E}-04$	$4.941\text{E}-06 \pm 1.759\text{E}-04$	$8.129\text{E}-04 \pm 4.902\text{E}-04$
20180530	$-9.789\text{E}-05 \pm 7.637\text{E}-05$	$1.044\text{E}-04 \pm 1.278\text{E}-04$	$-4.850\text{E}-04 \pm 1.784\text{E}-04$	$1.443\text{E}-04 \pm 4.982\text{E}-04$

Table 4. Results for the 8×72 -day sets

Start Date of set	$\Delta R_{Cz}/R_{\odot}$					
	a_2	a_4	a_6	a_8		
GONG						
19950718	$-2.768E-05 \pm 1.121E-04$	$5.896E-07 \pm 1.862E-04$	$4.227E-04 \pm 2.477E-04$	$-2.671E-04 \pm 5.791E-04$		
19960501	$-1.740E-04 \pm 1.078E-04$	$-8.954E-04 \pm 1.813E-04$	$-9.408E-04 \pm 2.446E-04$	$-6.814E-04 \pm 5.705E-04$		
19970213	$1.695E-06 \pm 1.036E-04$	$-2.947E-04 \pm 1.682E-04$	$-6.202E-05 \pm 2.302E-04$	$-1.127E-04 \pm 5.302E-04$		
19971128	$-2.398E-06 \pm 1.025E-04$	$4.251E-04 \pm 1.717E-04$	$1.401E-04 \pm 2.354E-04$	$-5.582E-04 \pm 5.335E-04$		
19980912	$-1.036E-04 \pm 1.042E-04$	$5.010E-04 \pm 1.676E-04$	$-1.571E-04 \pm 2.347E-04$	$2.426E-04 \pm 5.557E-04$		
19990627	$-9.036E-05 \pm 1.069E-04$	$-7.658E-04 \pm 1.747E-04$	$-3.574E-04 \pm 2.406E-04$	$-8.071E-04 \pm 5.870E-04$		
20000410	$-7.886E-05 \pm 1.030E-04$	$3.777E-04 \pm 1.675E-04$	$-2.984E-06 \pm 2.337E-04$	$2.935E-04 \pm 5.651E-04$		
20010123	$-2.371E-04 \pm 1.019E-04$	$2.336E-04 \pm 1.668E-04$	$2.481E-04 \pm 2.289E-04$	$6.042E-04 \pm 5.790E-04$		
20011107	$7.796E-05 \pm 9.848E-05$	$-3.725E-04 \pm 1.656E-04$	$-6.139E-04 \pm 2.302E-04$	$-1.621E-05 \pm 5.961E-04$		
20020822	$1.382E-04 \pm 9.195E-05$	$1.558E-04 \pm 1.596E-04$	$-1.240E-04 \pm 2.159E-04$	$-9.486E-04 \pm 5.505E-04$		
20030606	$4.546E-04 \pm 9.708E-05$	$-2.729E-04 \pm 1.606E-04$	$-4.267E-05 \pm 2.180E-04$	$2.217E-05 \pm 5.547E-04$		
20040320	$-5.259E-05 \pm 9.476E-05$	$-4.382E-04 \pm 1.549E-04$	$-1.462E-03 \pm 2.164E-04$	$2.752E-04 \pm 5.265E-04$		
20050102	$-3.309E-04 \pm 9.830E-05$	$-1.548E-04 \pm 1.611E-04$	$-5.587E-04 \pm 2.261E-04$	$3.355E-04 \pm 5.552E-04$		
20051017	$-2.970E-05 \pm 1.003E-04$	$4.462E-04 \pm 1.667E-04$	$-7.517E-04 \pm 2.292E-04$	$6.905E-04 \pm 5.653E-04$		
20060801	$-5.539E-05 \pm 1.009E-04$	$4.082E-05 \pm 1.709E-04$	$-2.453E-04 \pm 2.309E-04$	$-2.289E-04 \pm 5.714E-04$		
20070516	$-4.547E-04 \pm 9.964E-05$	$2.595E-04 \pm 1.663E-04$	$-7.486E-05 \pm 2.259E-04$	$1.291E-04 \pm 5.659E-04$		
20080228	$-4.131E-04 \pm 1.005E-04$	$-8.335E-04 \pm 1.720E-04$	$1.025E-03 \pm 2.331E-04$	$1.958E-03 \pm 5.736E-04$		
20081212	$3.793E-04 \pm 1.002E-04$	$-6.164E-04 \pm 1.647E-04$	$6.337E-04 \pm 2.261E-04$	$-9.614E-04 \pm 5.635E-04$		
20090926	$1.014E-04 \pm 9.360E-05$	$4.171E-04 \pm 1.573E-04$	$-3.940E-04 \pm 2.151E-04$	$1.164E-04 \pm 5.285E-04$		
20100711	$3.666E-04 \pm 9.888E-05$	$1.948E-04 \pm 1.608E-04$	$1.967E-05 \pm 2.228E-04$	$1.424E-03 \pm 5.518E-04$		
20110425	$3.511E-04 \pm 9.564E-05$	$-3.026E-04 \pm 1.563E-04$	$4.268E-04 \pm 2.187E-04$	$4.378E-04 \pm 5.429E-04$		
20120207	$2.882E-04 \pm 9.331E-05$	$2.004E-04 \pm 1.564E-04$	$9.971E-04 \pm 2.156E-04$	$8.493E-06 \pm 5.303E-04$		
20121121	$-1.074E-04 \pm 9.441E-05$	$1.453E-04 \pm 1.572E-04$	$2.014E-04 \pm 2.152E-04$	$1.176E-04 \pm 5.446E-04$		
20130905	$-2.840E-04 \pm 9.456E-05$	$-7.684E-04 \pm 1.584E-04$	$-3.281E-04 \pm 2.160E-04$	$-4.680E-04 \pm 5.513E-04$		
20140620	$-1.505E-04 \pm 9.491E-05$	$-5.927E-04 \pm 1.566E-04$	$3.403E-05 \pm 2.193E-04$	$2.929E-04 \pm 5.468E-04$		
20150404	$-1.182E-04 \pm 9.221E-05$	$-3.787E-04 \pm 1.523E-04$	$8.066E-05 \pm 2.127E-04$	$-1.006E-03 \pm 5.242E-04$		
20160117	$1.371E-04 \pm 9.953E-05$	$-2.947E-04 \pm 1.642E-04$	$-1.361E-04 \pm 8.816E-05$	$-7.683E-04 \pm 5.628E-04$		
20161031	$-7.077E-06 \pm 9.976E-05$	$2.267E-04 \pm 1.658E-04$	$3.942E-04 \pm 2.248E-04$	$1.029E-03 \pm 5.638E-04$		
20170815	$7.155E-05 \pm 1.019E-04$	$6.435E-04 \pm 1.672E-04$	$5.155E-04 \pm 2.345E-04$	$1.014E-03 \pm 5.626E-04$		
20180530	$-1.711E-04 \pm 1.031E-04$	$6.856E-04 \pm 1.710E-04$	$-2.455E-04 \pm 2.409E-04$	$3.270E-06 \pm 5.821E-04$		
20190314	$-1.832E-04 \pm 1.026E-04$	$5.598E-04 \pm 1.703E-04$	$-1.281E-04 \pm 2.407E-04$	$2.135E-04 \pm 5.726E-04$		
20191227	$-1.297E-04 \pm 1.017E-04$	$-2.802E-04 \pm 1.699E-04$	$-2.404E-04 \pm 2.363E-04$	$8.210E-04 \pm 5.696E-04$		
20201010	$-9.323E-05 \pm 1.017E-04$	$-5.041E-04 \pm 1.701E-04$	$1.027E-04 \pm 2.334E-04$	$-7.132E-04 \pm 5.813E-04$		
MDI						
19960501	$-1.679E-04 \pm 3.243E-05$	$-6.696E-04 \pm 1.995E-04$	$-1.122E-04 \pm 2.893E-04$	$4.351E-04 \pm 7.790E-04$		
19970213	$-8.866E-05 \pm 1.185E-04$	$-1.727E-04 \pm 1.990E-04$	$-6.224E-05 \pm 2.829E-04$	$-4.827E-04 \pm 7.841E-04$		
19971128	$-2.465E-04 \pm 1.566E-04$	$3.129E-04 \pm 2.105E-04$	$1.275E-05 \pm 2.979E-04$	$-1.032E-03 \pm 8.467E-04$		
19980912	$-2.922E-04 \pm 1.198E-04$	$-2.801E-04 \pm 1.999E-04$	$-8.307E-04 \pm 2.939E-04$	$-5.026E-04 \pm 8.066E-04$		
19990627	$1.646E-04 \pm 1.166E-04$	$-8.052E-04 \pm 1.975E-04$	$-8.777E-04 \pm 2.783E-04$	$-3.687E-05 \pm 7.673E-04$		
20000410	$1.817E-04 \pm 1.176E-04$	$4.883E-04 \pm 1.907E-04$	$1.037E-04 \pm 2.718E-04$	$8.150E-04 \pm 7.486E-04$		
20010123	$-1.237E-04 \pm 1.132E-04$	$5.303E-04 \pm 1.885E-04$	$1.721E-04 \pm 2.701E-04$	$9.066E-04 \pm 7.568E-04$		
20011107	$1.415E-04 \pm 1.136E-04$	$-1.612E-04 \pm 1.935E-04$	$-4.518E-04 \pm 2.736E-04$	$6.942E-05 \pm 7.623E-04$		
20020822	$2.985E-04 \pm 1.139E-04$	$1.852E-04 \pm 1.876E-04$	$-6.602E-04 \pm 2.712E-04$	$-1.729E-03 \pm 7.419E-04$		
20030606	$3.188E-04 \pm 1.124E-04$	$-3.285E-04 \pm 1.881E-04$	$-3.241E-04 \pm 2.704E-04$	$-1.118E-03 \pm 7.515E-04$		
20040320	$6.623E-05 \pm 1.138E-04$	$-3.604E-04 \pm 1.832E-04$	$-8.670E-04 \pm 2.714E-04$	$1.889E-04 \pm 7.413E-04$		
20050102	$-2.914E-04 \pm 1.182E-04$	$-1.887E-04 \pm 1.905E-04$	$-3.699E-04 \pm 2.837E-04$	$5.695E-04 \pm 7.536E-04$		
20051017	$8.274E-05 \pm 1.172E-04$	$4.241E-04 \pm 1.966E-04$	$-7.149E-04 \pm 2.828E-04$	$7.244E-04 \pm 8.036E-04$		
20060801	$-1.746E-04 \pm 1.259E-04$	$-1.810E-04 \pm 1.966E-04$	$-5.586E-04 \pm 2.922E-04$	$3.703E-05 \pm 7.920E-04$		
20070516	$-3.081E-04 \pm 1.235E-04$	$4.014E-04 \pm 2.011E-04$	$-4.883E-04 \pm 3.002E-04$	$-5.064E-04 \pm 8.360E-04$		
20080228	$-3.176E-04 \pm 1.261E-04$	$-3.337E-04 \pm 2.074E-04$	$8.664E-04 \pm 3.022E-04$	$6.559E-04 \pm 8.489E-04$		
20081212	$3.450E-04 \pm 1.265E-04$	$-8.905E-04 \pm 2.091E-04$	$3.180E-04 \pm 3.004E-04$	$-1.078E-03 \pm 8.400E-04$		
HMI						
20100711	$2.960E-04 \pm 1.005E-04$	$-9.257E-05 \pm 1.687E-04$	$7.059E-05 \pm 2.342E-04$	$6.507E-04 \pm 6.662E-04$		
20110425	$3.035E-04 \pm 9.867E-05$	$-3.076E-04 \pm 1.622E-04$	$6.568E-04 \pm 2.388E-04$	$1.052E-03 \pm 6.354E-04$		
20120207	$2.004E-04 \pm 9.656E-05$	$2.827E-04 \pm 1.613E-04$	$1.092E-03 \pm 2.259E-04$	$1.454E-04 \pm 5.285E-05$		
20121121	$2.966E-05 \pm 9.677E-05$	$2.004E-04 \pm 1.602E-04$	$4.489E-04 \pm 2.236E-04$	$-1.435E-04 \pm 6.175E-04$		
20130905	$-1.784E-04 \pm 9.671E-05$	$-8.528E-04 \pm 1.614E-04$	$-5.878E-04 \pm 2.201E-04$	$1.844E-04 \pm 6.199E-04$		
20140620	$2.003E-05 \pm 9.364E-05$	$-5.574E-04 \pm 1.646E-04$	$-8.529E-05 \pm 2.323E-04$	$5.331E-04 \pm 6.363E-04$		
20150404	$-8.478E-05 \pm 9.577E-05$	$-3.624E-04 \pm 1.616E-04$	$-1.534E-05 \pm 2.305E-04$	$-6.690E-04 \pm 6.253E-04$		
20160117	$2.328E-04 \pm 1.001E-04$	$-2.673E-04 \pm 1.685E-04$	$4.211E-04 \pm 2.341E-04$	$-2.158E-04 \pm 6.560E-04$		
20161031	$1.006E-04 \pm 1.021E-04$	$1.180E-04 \pm 1.744E-04$	$2.347E-04 \pm 2.401E-04$	$1.175E-03 \pm 6.647E-04$		
20170815	$9.367E-05 \pm 1.057E-04$	$1.250E-04 \pm 1.735E-04$	$3.774E-04 \pm 2.456E-04$	$1.029E-03 \pm 6.871E-04$		
20180530	$-1.398E-04 \pm 1.079E-04$	$5.611E-04 \pm 1.824E-04$	$-4.173E-04 \pm 2.494E-04$	$-2.271E-04 \pm 7.161E-04$		
20190314	$-9.100E-05 \pm 1.120E-04$	$4.868E-04 \pm 1.874E-04$	$-8.267E-06 \pm 2.726E-04$	$8.871E-05 \pm 7.282E-04$		
20191227	$-1.880E-04 \pm 1.035E-04$	$5.511E-05 \pm 1.711E-04$	$-3.143E-04 \pm 2.511E-04$	$3.282E-04 \pm 6.994E-04$		
20201010	$1.053E-04 \pm 1.014E-04$	$-3.848E-04 \pm 1.690E-04$	$2.648E-05 \pm 2.373E-04$	$-1.121E-03 \pm 6.684E-04$		

Table 5. Results for the 5×72 -day sets

Start Date of set	$\Delta R_{Cz}/R_{\odot}$			
	a_2	a_4	a_6	a_8
GONG				
19960501	$-3.588E-05 \pm 1.319E-04$	$-9.555E-04 \pm 2.174E-04$	$-1.704E-03 \pm 3.081E-04$	$2.839E-04 \pm 7.079E-04$
19970426	$5.235E-05 \pm 1.254E-04$	$-2.939E-04 \pm 2.077E-04$	$3.811E-04 \pm 2.894E-04$	$-3.486E-04 \pm 6.605E-04$
19980421	$-2.454E-04 \pm 1.224E-04$	$4.944E-04 \pm 1.958E-04$	$-2.373E-04 \pm 2.715E-04$	$-3.828E-04 \pm 6.463E-04$
19990416	$-3.982E-04 \pm 1.248E-04$	$-7.308E-05 \pm 2.007E-04$	$4.238E-04 \pm 2.924E-04$	$1.002E-03 \pm 6.957E-04$
20000410	$3.672E-04 \pm 1.254E-04$	$3.735E-04 \pm 2.032E-04$	$-9.070E-04 \pm 2.842E-04$	$-3.152E-04 \pm 6.923E-04$
20010405	$-2.928E-04 \pm 1.199E-04$	$-4.916E-05 \pm 1.961E-04$	$2.728E-04 \pm 2.752E-04$	$9.851E-04 \pm 6.963E-04$
20020331	$-1.104E-04 \pm 1.232E-04$	$-4.174E-04 \pm 1.926E-04$	$-1.592E-03 \pm 2.699E-04$	$-8.070E-04 \pm 6.928E-04$
20030326	$2.632E-04 \pm 1.083E-04$	$4.787E-04 \pm 1.849E-04$	$8.017E-04 \pm 2.524E-04$	$-1.207E-03 \pm 6.362E-04$
20040320	$7.737E-05 \pm 1.132E-04$	$-5.069E-04 \pm 1.866E-04$	$-1.369E-03 \pm 2.646E-04$	$9.853E-04 \pm 6.463E-04$
20050315	$-5.549E-04 \pm 1.141E-04$	$8.013E-04 \pm 1.935E-04$	$-1.379E-03 \pm 2.636E-04$	$5.958E-04 \pm 6.638E-04$
20060310	$2.420E-04 \pm 1.196E-04$	$1.808E-04 \pm 2.008E-04$	$-3.567E-04 \pm 2.713E-04$	$9.843E-04 \pm 6.710E-04$
20070305	$1.442E-05 \pm 1.206E-04$	$6.549E-04 \pm 1.963E-04$	$-6.800E-04 \pm 2.784E-04$	$-5.827E-04 \pm 6.745E-04$
20080228	$-9.281E-04 \pm 1.246E-04$	$-4.970E-04 \pm 2.050E-04$	$-2.762E-04 \pm 2.874E-04$	$1.660E-03 \pm 6.899E-04$
20090222	$-1.614E-04 \pm 1.193E-04$	$-1.082E-03 \pm 2.054E-04$	$1.009E-03 \pm 2.777E-04$	$4.417E-04 \pm 6.982E-04$
20100217	$4.107E-04 \pm 1.185E-04$	$3.724E-04 \pm 1.983E-04$	$-2.199E-04 \pm 2.767E-04$	$2.806E-04 \pm 6.732E-04$
20110212	$2.066E-04 \pm 1.129E-04$	$-1.228E-04 \pm 1.814E-04$	$-3.439E-04 \pm 2.537E-04$	$1.859E-03 \pm 6.089E-04$
20120207	$4.621E-04 \pm 1.126E-04$	$2.408E-05 \pm 1.842E-04$	$1.372E-03 \pm 2.652E-04$	$-1.059E-04 \pm 6.187E-05$
20130201	$3.435E-04 \pm 1.105E-04$	$-1.916E-04 \pm 1.863E-04$	$3.637E-04 \pm 2.588E-04$	$-2.188E-04 \pm 6.373E-04$
20140127	$-6.314E-04 \pm 1.101E-04$	$-5.387E-04 \pm 1.837E-04$	$-1.264E-03 \pm 2.585E-04$	$-1.069E-03 \pm 6.439E-04$
20150122	$-2.463E-04 \pm 1.116E-04$	$-6.898E-04 \pm 1.846E-04$	$8.648E-04 \pm 2.553E-04$	$3.754E-04 \pm 6.317E-04$
20160117	$-4.519E-05 \pm 1.129E-04$	$-5.044E-05 \pm 1.867E-04$	$3.817E-04 \pm 2.592E-04$	$-1.344E-03 \pm 6.463E-04$
20170111	$2.313E-04 \pm 1.156E-04$	$3.874E-04 \pm 1.969E-04$	$-9.711E-04 \pm 2.686E-04$	$1.930E-03 \pm 6.802E-04$
20180106	$2.746E-06 \pm 1.232E-04$	$7.786E-04 \pm 2.075E-04$	$-4.994E-05 \pm 2.776E-04$	$3.548E-04 \pm 6.902E-04$
20190101	$-1.264E-04 \pm 1.227E-04$	$8.592E-04 \pm 2.064E-04$	$1.348E-05 \pm 2.897E-04$	$-2.098E-03 \pm 7.146E-04$
20191227	$9.851E-05 \pm 1.184E-04$	$2.520E-04 \pm 8.238E-05$	$-5.347E-04 \pm 2.786E-04$	$1.272E-03 \pm 6.917E-04$
20201221	$1.857E-04 \pm 1.194E-04$	$-7.613E-04 \pm 1.960E-04$	$-4.214E-04 \pm 2.781E-04$	$-1.551E-04 \pm 6.788E-04$
MDI				
19960501	$-3.249E-05 \pm 1.496E-04$	$-6.739E-04 \pm 2.465E-04$	$-5.510E-04 \pm 3.652E-04$	$6.758E-04 \pm 1.002E-03$
19970426	$1.408E-04 \pm 1.413E-04$	$-8.259E-05 \pm 2.230E-04$	$8.475E-04 \pm 3.428E-04$	$2.433E-04 \pm 9.325E-04$
19980421	$-4.957E-04 \pm 1.669E-04$	$1.159E-03 \pm 2.623E-04$	$-1.588E-03 \pm 3.901E-04$	$-1.131E-03 \pm 1.081E-03$
19990416	$-6.330E-04 \pm 1.397E-04$	$-2.152E-04 \pm 2.252E-04$	$-5.035E-04 \pm 3.297E-04$	$1.589E-03 \pm 8.885E-04$
20000410	$4.040E-04 \pm 1.355E-04$	$5.631E-05 \pm 2.295E-04$	$-1.165E-03 \pm 3.199E-04$	$-2.085E-04 \pm 8.908E-04$
20010405	$-3.047E-04 \pm 1.399E-04$	$5.622E-04 \pm 2.298E-04$	$-3.100E-04 \pm 3.347E-04$	$6.868E-04 \pm 9.124E-04$
20020331	$-1.789E-04 \pm 1.372E-04$	$-5.572E-04 \pm 2.242E-04$	$-1.441E-03 \pm 3.222E-04$	$-5.479E-04 \pm 8.969E-04$
20030326	$3.194E-04 \pm 2.223E-04$	$3.193E-04 \pm 2.273E-04$	$2.665E-04 \pm 3.130E-04$	$-8.599E-04 \pm 8.816E-04$
20040320	$2.402E-04 \pm 1.355E-04$	$-6.730E-04 \pm 2.291E-04$	$-7.335E-04 \pm 3.338E-04$	$-3.220E-04 \pm 9.001E-04$
20050315	$-3.596E-04 \pm 1.345E-04$	$-1.755E-04 \pm 2.169E-04$	$-1.810E-03 \pm 3.311E-04$	$-1.319E-04 \pm 9.100E-04$
20060310	$8.495E-05 \pm 1.465E-04$	$4.389E-05 \pm 2.351E-04$	$-2.662E-04 \pm 3.444E-04$	$8.014E-04 \pm 9.261E-04$
20070305	$-1.004E-05 \pm 1.484E-04$	$7.712E-04 \pm 2.398E-04$	$-6.664E-04 \pm 3.555E-04$	$-3.810E-04 \pm 9.607E-04$
20080228	$-1.021E-04 \pm 1.549E-04$	$1.166E-04 \pm 2.602E-04$	$-1.027E-03 \pm 3.755E-04$	$8.020E-04 \pm 1.028E-03$
20090222	$2.454E-04 \pm 1.513E-04$	$-1.410E-04 \pm 2.515E-04$	$3.212E-04 \pm 3.520E-04$	$1.850E-04 \pm 9.895E-04$
20100217	$4.135E-04 \pm 1.466E-04$	$6.335E-04 \pm 2.361E-04$	$1.217E-05 \pm 3.362E-04$	$1.275E-04 \pm 9.530E-04$
HMI				
20110212	$2.221E-04 \pm 1.158E-04$	$-3.019E-04 \pm 1.966E-04$	$-3.283E-05 \pm 2.749E-04$	$5.365E-04 \pm 7.576E-04$
20120207	$8.597E-05 \pm 1.199E-04$	$-2.730E-04 \pm 2.011E-04$	$1.516E-03 \pm 2.815E-04$	$1.766E-04 \pm 7.678E-04$
20130201	$3.320E-04 \pm 1.133E-04$	$-3.490E-04 \pm 1.913E-04$	$3.782E-04 \pm 2.728E-04$	$-5.435E-04 \pm 7.725E-04$
20140127	$-4.768E-04 \pm 1.144E-04$	$-5.917E-04 \pm 1.920E-04$	$-1.209E-03 \pm 2.717E-04$	$4.920E-04 \pm 7.298E-04$
20150122	$-2.282E-04 \pm 1.143E-04$	$-8.276E-04 \pm 1.904E-04$	$4.310E-04 \pm 2.738E-04$	$3.211E-04 \pm 7.434E-04$
20160117	$-1.630E-05 \pm 1.192E-04$	$2.743E-05 \pm 1.970E-04$	$2.686E-04 \pm 2.685E-04$	$-8.003E-04 \pm 7.849E-04$
20170111	$5.495E-05 \pm 1.165E-04$	$3.503E-04 \pm 2.067E-04$	$-8.565E-04 \pm 2.853E-04$	$1.195E-03 \pm 7.689E-04$
20180106	$1.701E-04 \pm 1.305E-04$	$1.054E-04 \pm 2.117E-04$	$-2.592E-04 \pm 2.929E-04$	$4.161E-04 \pm 8.183E-04$
20190101	$-1.138E-04 \pm 1.274E-04$	$6.896E-04 \pm 2.201E-04$	$3.924E-04 \pm 3.210E-04$	$-1.611E-03 \pm 8.639E-04$
20191227	$2.661E-04 \pm 1.332E-04$	$-2.377E-04 \pm 2.241E-04$	$1.229E-04 \pm 3.164E-04$	$8.825E-04 \pm 8.766E-04$
20201221	$2.669E-04 \pm 1.245E-04$	$-3.865E-04 \pm 2.142E-04$	$-2.735E-04 \pm 3.101E-04$	$-5.221E-04 \pm 8.384E-04$